Spectral intensities and frequencies of spin waves in ferromagnetic cylinders: Application to nickel nanowires

T. M. Nguyen and M. G. Cottam
Department of Physics and Astronomy, University of Western Ontario, London, Ontario, Canada N6A 3K7
(Received 12 July 2005; published 12 December 2005)

The theory for dipole-exchange spin waves in cylindrical ferromagnetic nanowires, as developed in a previous paper, is extended to include spectral intensities, arbitrary orientation of external magnetic field, and effects of single-ion anisotropy. This allows applications to be made to the nickel nanowires studied experimentally. The dependences of the spin-wave frequencies on the nanowire radius, wave vector, and magnetic field are investigated, and the spatial distribution of the eigenmodes are evaluated to analyze their localization. The spectral intensities are calculated within a Green's function formalism, giving a good insight into data from Brillouin light scattering. The spin-wave frequencies obtained in the case of zero field are compared to the experimental results for nickel, and to results deduced from macroscopic theory under conditions of small surface pinning. Also when the magnetic field is perpendicular to the wire axis, making the magnetization nonuniform, our results provide a good description of the experimental behavior.

DOI: 10.1103/PhysRevB.72.224415 PACS number(s): 75.30.Ds, 75.75.+a

I. INTRODUCTION

Submicrometer-scale magnetic systems have been fabricated and studied extensively in various geometries, such as arrays of wires, dots, rings, etc. This has been done from the point of view of both novel fundamental physics and promising applications in advanced magnetic devices. Understanding the static and dynamical properties of these systems has been the main objective of recent experimental and theoretical works (see, e.g., Refs 1–8). Among the systems studied extensively, arrays of nickel nanowires have attracted attention due to the elegant method for fabricating these systems by electrodeposition into templates compared to other lithography-based methods.[2,5,6] Interest in these systems has focused on static properties, magnetization dynamics, and giant magnetoresistance, to name but a few. Recently, it was found that magnetic nanowires can be bound to cells and some biomolecules, and are therefore applicable in biology and biotechnology.[9]

In this paper we focus our attention on the magnetic excitations, namely, spin waves (SWs), in nickel nanowires of *approximately* circular cross section. Understanding the spin dynamics, via the SW excitations, in any magnetic system is important because they govern the low-temperature behavior. Also, from SW measurements, one may deduce fundamental properties, such as the exchange stiffness, the distribution of the internal field, the magnetic anisotropy, strength of dipolar interactions, etc. The SW behavior can also provide an indicator for a phase transition (or spin reorientation) within the system.

Specially we employ a microscopic theory for SWs in ferromagnetic nanowires, concentrating on the regime where both exchange and dipolar interactions may provide comparable contributions to the dynamical processes. An objective is to make realistic applications to Brillouin light scattering from metallic nanowires as reported recently for nickel arrays[10] with wire diameters in the range 25 to 55 nm, i.e., larger than the so-called exchange length of order 2–3 nm in Ni. The theory is developed by extending our recent theory[11] to include the spectral intensities of the SW (as well as the frequencies), surface anisotropy, and arbitrary orientation of the external magnetic field. The Green's function method that we employ here in making these extension is analogous to that developed in recent work on ultrathin films of ferromagnets[12] and antiferromagnets.[13] Comparisons are also made with previous macroscopic (continuum) theories, applicable only for longitudinal external magnetic field, using magnetostatic[14] and dipole-exchange[15] methods.

The paper is arranged as follows. Section II describes the theoretical model applied to cylindrical ferromagnetic nanowires. The Hamiltonian includes the exchange, dipolar, anisotropy, and Zeeman terms, where the external magnetic field is applied at an arbitrary angle to the nanowire axis. Results for linear SW dispersion relation are then derived in Sec. III, where numerical examples are provided to illustrate the theory for the dependence of the discrete SW frequencies on nanowire radius, wave vector, and applied magnetic field. Numerical results are included for the spatial distribution of the modes as well as the spectral intensities. Section IV is devoted to further discussion and overall conclusions.

II. LINEAR SPIN-WAVE ANALYSIS

We consider a microscopic model for single ferromagnetic nanowires, as described in our previous paper.[11] Briefly, each cross section of the wire is represented by a hexagon with the spins arranged on a triangular lattice (with spacing a). The total number of spins N in each cross-section layer is $3r(r+1)+1$ for $r=0, 1, 2,\ldots$, where the wire "radius" is ra. The layers are then stacked vertically along the y axis (see Fig. 1 of Ref. 11) to form a wire. The system is described by the spin Hamiltonian

$$H = -\frac{1}{2}\sum_{in,jm} J_{in,jm}\mathbf{S}_{in}\cdot\mathbf{S}_{jm} + \frac{1}{2}g^2\mu_B^2\sum_{in,jm}\sum_{\alpha,\beta} D^{\alpha,\beta}_{in,jm}S^{\alpha}_{in}S^{\beta}_{jm} - g\mu_B\sum_{in}\mathbf{H}_n\cdot\mathbf{S}_{in}. \quad (1)$$

Here i, j are indices for the layers, while n, m label the

position of the spins in a particular layer. The exchange interaction between the spin operators at sites (i,n) and (j,m) is $J_{in,jm}$. The second term in Eq. (1) describes the long-range dipole-dipole interactions with the α and β labels denoting Cartesian components x, y, or z, and

$$D_{in,jm}^{\alpha,\beta} = \frac{|\mathbf{r}_{in,jm}|^2 \delta_{\alpha,\beta} - 3r_{in,jm}^{\alpha} r_{in,jm}^{\beta}}{|\mathbf{r}_{in,jm}|^5}, \tag{2}$$

where $\mathbf{r}_{in,jm}=(x_m-x_n, y_j-y_i, z_m-z_n)$, and the equal-site case $(i=j, n=m)$ is excluded from the sums in Eq. (1). Generalizing Ref. 11, the final term in Eq. (1) represents the combined effect of the Zeeman energy due to an external magnetic field and the single-ion anisotropy. We take the external field to be in the yz plane, so $\mathbf{H}_0=(0,H_{\parallel},H_{\perp})$, while the anisotropy is represented here in terms of an effective field $\mathbf{H}_{an}$ which may be site dependent. This approximation should be satisfactory provided the single-ion anisotropy is uniaxial (with our y axis as the prefered direction) and the sample is magnetized along the y direction. More generally, we might write the anisotropy term as $-K_n(S_{in}^y)^2$ at each site. In the uniaxial case (where coefficient $K_n>0$) with a longitudinal applied field, the correspondence between the two forms is well known to be approximately $H_{an}^y=2\langle S_{in}^y\rangle K_n$. We do not include the case of "easy-plane" anisotropy (where $K_n<0$) in the present work.

Generally, the magnetization of the system is inhomogeneous due to the interplay between the applied field and the demagnetizing fields. The equilibrium configuration of spins is found by optimizing the total free energy of the system, following the method described in Ref. 11. The equilibrium orientation of a spin at site (i,n) is then represented by two angles $\{\alpha_n, \theta_n\}$ in polar coordinates (see Fig. 1b of Ref. 11). The linear SWs at low temperatures $(T \ll T_c)$ are investigated by the Green's function method, following Refs. 11–13. We first use the Holstein-Primakoff transformation to convert the spin Hamiltonian into an equivalent form in boson operators. The transformation is applied with respect to the *local* coordinates (x',y',z'), which are assigned to each spin individually such that the y' axis is along the equilibrium direction of that spin. Corresponding to our choice of coordinate axes, the components of the spin vector $\mathbf{S}_{in}$ are represented in terms of boson creation and annihilation operators $a_{in}^{\dagger}$ and a_{in} by the expressions (denoting $S_{in}^{\pm}=S_{in}^{z'}\pm iS_{in}^{x'}$)

$$S_{in}^{+} = \sqrt{2S}(1 - a_{in}^{\dagger}a_{in}/2S)^{1/2} a_{in}, \tag{3}$$

$$S_{in}^{-} = \sqrt{2S} a_{in}^{\dagger}(1 - a_{in}^{\dagger}a_{in}/2S)^{1/2}, \tag{4}$$

$$S_{in}^{y'} = S - a_{in}^{\dagger}a_{in}. \tag{5}$$

The transformation relating the global coordinates (x,y,z) to the local coordinates has the following form:

$$\begin{pmatrix} S_{in}^{x} \\ S_{in}^{y} \\ S_{in}^{z} \end{pmatrix} = \begin{pmatrix} \cos\theta_n & \sin\theta_n \sin\alpha_n & \sin\theta_n \cos\alpha_n \\ 0 & \cos\alpha_n & -\sin\alpha_n \\ -\sin\theta_n & \cos\theta_n \sin\alpha_n & \cos\theta_n \cos\alpha_n \end{pmatrix} \begin{pmatrix} S_{in}^{x'} \\ S_{in}^{y'} \\ S_{in}^{z'} \end{pmatrix}. \tag{6}$$

We now substitute the above transformation into the Hamiltonian (1), which can be expanded in terms of boson operators as $H=E+H^{(2)}+H^{(3)}+H^{(4)}\cdots$, where $H^{(m)}$ denotes a term with m boson operators. The first-order term $H^{(1)}$ is found to vanish due to the minimization of the energy E, and the noninteracting (linear) SW excitations can be obtained from the quadratic Hamiltonian $H^{(2)}$. After making a one-dimensional (1D) Fourier transform along the wire axis, it has the form

$$H^{(2)} = \sum_{k,n,m} \{A_{n,m}^{(2)}(k) a_{k,n}^{\dagger} a_{k,m} + B_{n,m}^{(2)}(k) a_{k,n}^{\dagger} a_{-k,m}^{\dagger} + B_{n,m}^{(2)*}(k) a_{k,n} a_{-k,m}\}, \tag{7}$$

where k is the wave number along the y axis of symmetry. The terms $H^{(3)}$ and $H^{(4)}$ describe the leading-order effects of SW interactions and will not be considered further in the present paper. The coefficients $A_{n,m}^{(2)}(k)$ and $B_{n,m}^{(2)}(k)$ depend on the canting angles $\{\alpha_n, \theta_n\}$ and are quoted in the Appendix . The boson operators $a_{k,n}^{\dagger}$ and $a_{k,m}$ are represented in terms of k and the site indices n and m in a particular layer.

In order to obtain the linear SW spectrum, the quadratic Hamiltonian (7) must be diagonalized. This can be done by applying a generalized Bogoliubov transformation as in our previous paper.[11] It was shown there that the diagonalized Hamiltonian has the form

$$H^{(2)} = -\frac{1}{2}\sum_{k} \mathrm{Tr}[\mathbf{A}(k)] + \frac{1}{2}\sum_{k,l=1}^{N} \omega_{k,l} + \sum_{k,l=1}^{N} \omega_{k,l} b_{k,l}^{\dagger} b_{k,l}, \tag{8}$$

where $\mathbf{A}(k)$ is the $N\times N$ matrix with elements given by $A_{n,m}^{(2)}$, and the new boson operators $b_{k,l}^{\dagger}$ and $b_{k,l}$, which satisfy the usual commutation relations, are defined by

$$a_{k,n} = \sum_{l=1}^{N} S_{n,l}(k) b_{k,l} + S_{n,l+N}(k) b_{-k,l}^{\dagger}, , \tag{9}$$

$$a_{-k,n}^{\dagger} = \sum_{l=1}^{N} S_{n+N,l}(k) b_{k,l} + S_{n+N,l+N}(k) b_{-k,l}^{\dagger}. \tag{10}$$

Here $S_{n,m}(k)$ is an element of the $2N\times 2N$ transformation matrix $\mathbf{S}_k$, which satisfies the following condition:

$$\mathbf{S}_k \begin{pmatrix} \mathbf{I} & \mathbf{0} \\ \mathbf{0} & -\mathbf{I} \end{pmatrix} \widetilde{\mathbf{S}}_k^{*} = \begin{pmatrix} \mathbf{I} & \mathbf{0} \\ \mathbf{0} & -\mathbf{I} \end{pmatrix}, \tag{11}$$

where $\mathbf{I}$ is the $N\times N$ unit matrix, and the tilde denotes a transpose. Then the lth column of the matrix $\mathbf{S}_k$, which we denote by $\mathbf{S}_l(k)$, as well as the noninteracting SW frequencies, which we denote by $\omega_{k,l}$, can be found by solving the following eigenvalue equation:

$$\begin{pmatrix} \mathbf{A}(k) & 2\mathbf{B}(k) \\ -2\mathbf{B}^{*}(-k) & -\widetilde{\mathbf{A}}(-k) \end{pmatrix} \mathbf{S}_l(k) = \pm\, \omega_{k,l} \mathbf{S}_l(k), \tag{12}$$

where $\mathbf{B}(k)$ is the $N\times N$ matrix with elements given by $B_{n,m}^{(2)}$. Also the + sign is taken for $l=1,\ldots,N$ and the − sign for $l=N+1,\ldots,2N$.

We note that information about the spatial distribution of relative intensities of the SW modes can be deduced using

the transformation matrix $\mathbf{S}_k$. More precisely, we introduce

$$P_n(\omega_{k,l}) = \sqrt{|S_{n,l}(k)|^2 + |S_{n+N,l}(k)|^2} \tag{13}$$

as defining a probability amplitude for the mode with frequency $\omega_{k,l}$ propagating along the nth spin line. As a measure of the spatial distribution of any mode it is useful also to consider here the quantity $D(r_s, \omega_{k,l})$, associated with the SW mode of frequency $\omega_{k,l}$ propagating on the shell of radius r_s (in the units of a), defined by

$$D(r_s, \omega_{k,l}) = \sum_{n}^{\text{shell}(r_s)} |P_n(\omega_{k,l})|^2, \tag{14}$$

where $r_s = 0, 1, \ldots, r$ with r denoting is the effective radius of the nanowire. The summation is over all sites in the shell with radius r_s.

We also want the relative intensities associated with the discrete SW frequencies. This information can be acquired from the Green's functions of the form $\langle\langle a_{k,n}; a^{\dagger}_{k,m}\rangle\rangle_{\omega}$ at frequency ω. These quantities are directly related to the correlation functions of the dynamical part of the spin operators, and therefore contain a full description of the dynamic behavior of the system.[16] We first calculate the Green's functions corresponding to the diagonalized Hamiltonian (8) by solving the corresponding equation of motion to obtain

$$\langle\langle b_{k,l}; b^{\dagger}_{k',l'}\rangle\rangle_{\omega} = \langle\langle b^{\dagger}_{k,l}; b_{k',l'}\rangle\rangle_{-\omega} = \frac{1}{2\pi}\frac{\delta_{kk'}\delta_{ll'}}{\omega - \omega_{k,l}}. \tag{15}$$

Using the transformations in Eqs. (9) and (10) we get

$$\langle\langle a_{k,n}; a^{\dagger}_{k,m}\rangle\rangle_{\omega} = \frac{1}{2\pi}\sum_{l=1}^{N}\left(\frac{S_{n,l}(k)S^{*}_{m,l}(k)}{\omega - \omega_{k,l}} - \frac{S_{n,l+N}(k)S^{*}_{m,l+N}(k)}{\omega + \omega_{k,l}}\right). \tag{16}$$

A Green's function, which can be related to the total fluctuation spectrum for the system, is then defined as

$$G(k,\omega) = \sum_{n=1}^{N}\langle\langle a_{k,n}; a^{\dagger}_{k,n}\rangle\rangle_{\omega} = \frac{1}{2\pi}\sum_{l=1}^{N}\left(\frac{G^{-}_{l}(k)}{\omega - \omega_{k,l}} - \frac{G^{+}_{l}(k)}{\omega + \omega_{k,l}}\right), \tag{17}$$

where

$$G^{-}_{l}(k) = \sum_{n=1}^{N} S_{n,l}(k)S^{*}_{n,l}(k), \tag{18}$$

$$G^{+}_{l}(k) = \sum_{n=1}^{N} S_{n,l+N}(k)S^{*}_{n,l+N}(k). \tag{19}$$

Finally the spectral intensity associated with each SW mode is obtained by using the fluctuation-dissipation theorem[16] and is defined as

$$F(k,\omega) = -2[1 + n(\omega)]\,\text{Im}\,G(k, \omega + i\epsilon), \tag{20}$$

where ϵ is a positive infinitesimal ($\epsilon \to 0$) and $n(\omega)$ is the Bose-Einstein distribution function $[\exp(\hbar\omega/k_BT) - 1]^{-1}$. For the room-temperature Brillouin scattering experiments[10] to be discussed later, we have $\hbar\omega \ll k_BT$ and so $n(\omega) \simeq k_BT/\hbar\omega$.

III. NUMERICAL CALCULATIONS

We now apply the theory, as described above, to the SW modes in ferromagnetic nickel nanowires. These provide a good case for numerical studies because high-quality arrays of nanowires have been fabricated (see, e.g., Refs. 5 and 6) and three low-frequency SW branches were measured using Brillouin light scattering (BLS).[10] The latter technique supplemented earlier ferromagnetic resonance (FMR) studies[7,8] on other samples. We concentrate on two different situations, the longitudinal and transverse cases, corresponding to the external magnetic field applied either parallel or perpendicular to the wire axis. The numerical calculations are carried out in term of the dimensionless parameters $h = g\mu_B H_0/SJ$, $\mathbf{h}_{an} = g\mu_B \mathbf{H}_{an}/SJ$, and $R_d = (g\mu_B)^2/Ja^3$. These characterize the external magnetic field and the single-ion anisotropy fields (relative to SJ), and the ratio between dipolar and exchange interaction strengths. Equivalently, starting from values for the magnetization M_s and the exchange stiffness D of the nanowires, we are able to deduce all the microscopic parameters for our model. Specifically, we have the relations $h = H_0a^2/D$, $R_d = M_sa^2/D$, and $SJ = g\mu_B D/a^2$. In the following calculations, we use $g\mu_B = 30.9$ GHz/T (corresponding to $g = 2.21$) for nickel,[17] and the single-ion anisotropy fields are either set to zero or are introduced phenomenologically.

In the study of nickel nanowires by BLS,[10] the magnetization M_s was deduced to be 0.0480 T, similar to the value for bulk nickel.[17] However, the exchange stiffness D was obtained by fitting the results for the measured SW frequencies at zero field with the macroscopic theory of dipole-exchange SWs.[15] In the case of small pinning the value of D was inferred to be 3.13 T nm^2, which is about one order of magnitude smaller than for bulk materials.[17] It is, therefore, appropriate that in our calculations we examine the effect of using different values of D, as well as the one reported in Ref. 10. We note that in our calculations, surface pinning can arise due to the total effective dipolar fields having a position dependence [e.g., terms in Eq. (A3)] as well as due to any surface anisotropy field. This feature of a nonuniform dipolar field causing pinning was recently pointed out for magnetic nanostructures.[18]

The experimental BLS data[10] covered two different cases, namely, the variation of SW frequencies with nanowire radius in zero applied magnetic field, and the dependence of SW frequencies on a magnetic field applied perpendicular to the wire axis. The parameters reported in Ref. 10 correspond to wave number $k = 0.041$ nm^{-1} together with the above values for M_s and D. The exchange length in this case is deduced to be $l_{ex} \simeq 2.27$ nm, and we discuss its role later. The nanowires used in the experiments have radii of 12.5, 15, 20, and 27.5 nm, which are all larger than the exchange length by a factor of 5 or more. This implies that a dipole-exchange theory is appropriate.

A. Zero applied field

We note first, in the case of zero applied field, that the macroscopic theory as developed by Arias and Mills[15] was

TABLE I. SW frequencies (in GHz) of a nickel nanowire with $R=15$ nm in zero applied field, modeled by choosing $N=127$, 217, and 331. Only the lowest few branches are considered, and comparisons are made with Eq. (21) and with experiment (Ref. 10).

SW branch	$N=127$	$N=217$	$N=331$	Approx. [Eq. (21)]	Expt.[10]
$\omega_{k,1}$	4.68	4.69	4.70	5.41	4.79
$\omega_{k,2}$	7.01	7.03	7.03		
$\omega_{k,3}$	10.56	10.64	10.68	9.54	10.16
$\omega_{k,4}$	11.46	11.74	11.91		
$\omega_{k,5}$	14.37	14.64	14.81	14.12	14.81
$\omega_{k,6}$	14.97	15.43	15.71		

used in Ref. 10 to provide a good fit to the experimental data. The approximate SW frequency (taking $k \simeq 0$ and small pinning) employed by Wang *et al.* to fit their data for a wire of radius R is

$$\omega_l = g\mu_B\{D(a_l/R)^2[D(a_l/R)^2 + 4\pi M_s]\}^{1/2} \qquad (21)$$

where $l(=1,2,3,\ldots)$ plays the role of an azimuthal quantum number and enumerates the modes. The lowest three values of the constant a_l are $a_1=1.84$, $a_2=3.05$, and $a_3=4.20$.

As discussed in our previous paper,[11] the spin **S** at each "lattice" site may be chosen to represent either a single spin or a "cluster" of spins, in which case the lattice constant a used in our model is an effective value. Therefore we have some flexibility in the way of microscopically modelling a nanowire of given radius R. We note that $R=ra$ where r is the radial factor defined in Sec. II and related to the total number N of spins in any cross section. One constraint is that the "lattice constant" a should be chosen such that it is less than the exchange length, which is defined as $l_{ex}=(D/4\pi M_s)^{1/2}$. Within the scale of this exchange length, the spins deviate only slightly from one to another and can be treated as uniform and represented by an overall effective spin. Obviously, for a nanowire of given R, one expects to obtain better results by choosing smaller a and larger r, within the limitations imposed by computational resourses. It is evident that r and N must be large enough (and a small enough) that the predicted results for the SW properties do not depend on the precise choice of these parameters. To test for these effects we have carried out calculations for different sets of r and a values. In Table I we show the predicted results of the SW frequencies for a nanowire of radius $R=15$ nm modeled by three different choices. These are for $N=127$, 217, and 331, corresponding to the sets of values ($r=6$, $a=2.5$ nm), ($r=8$, $a=1.875$ nm), and ($r=10$, $a=1.5$ nm), respectively. Here the external magnetic field and the single-ion anisotropy are set to be zero, and only the six lowest modes are presented. Other parameters are taken from Ref. 10. The results corresponding to different choices of N are seen to be close to each other for these low-frequency SW modes, implying that it is good enough to choose $r=10$ and vary a to model nanowires of radius less than about 25 nm, as mostly used in the experiments. For nanowires of larger radius, one would need to increase the value of r (and N). Table I also shows how our results for

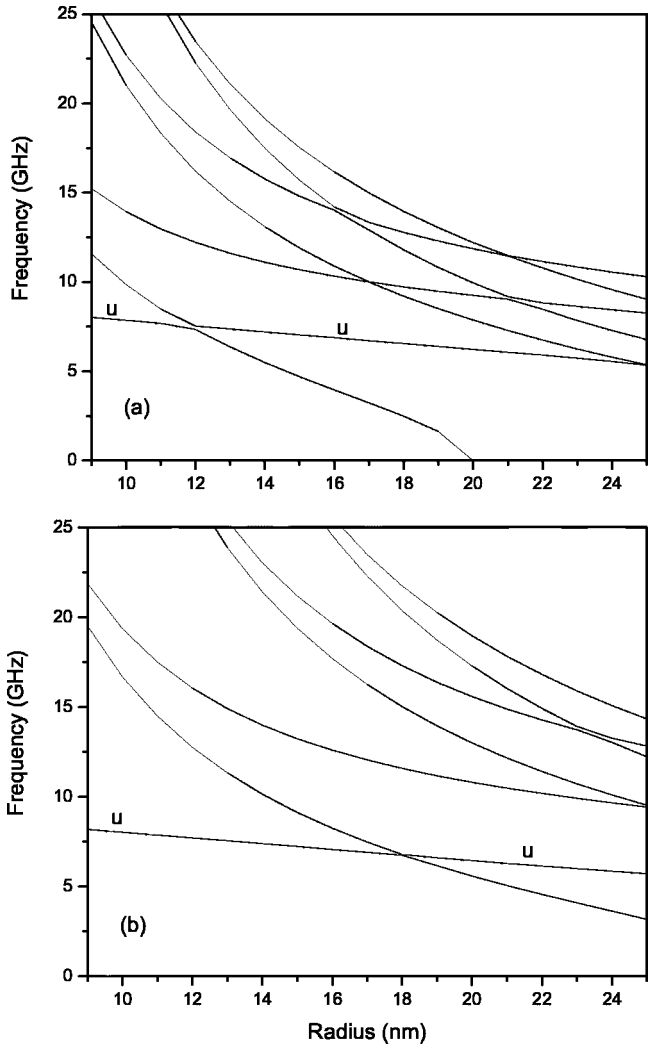

FIG. 1. SW frequency versus nanowire radius in zero applied magnetic field and zero anisotropy field, taking D= (a) 3.13 and (b) 6.26 T nm^2.

$R=15$ nm compare with the approximation of Eq. (21) and with experiment. Note that the second mode $\omega_{k,2}$ is identified as the uniform mode (as we discuss later). Its amplitude is distributed approximately uniformly thoughout the nanowire, implying that this mode does not interact with light and therefore is not observed using BLS. The third and fourth discrete modes are relatively close together in frequency and we surmise that (when linewidth effects are taken into account) they lead to only one peak in the spectral intensities. Similar arguments apply for the fifth and sixth modes. Justification for this is discussed later, and tentatively we identify the combined effect of these four modes with the second and the third peaks observed in the experiments,[10] respectively.

In Fig. 1(a) we show results for the SW frequencies versus nanowire radius in the case of no applied magnetic field and no single-ion anisotropy, using the same parameters as in Ref. 10. The nanowires are modeled by choosing $r=10$ (or $N=331$) and taking a to range from 0.9 to 2.5 nm. When we compare the results for nanowires of radius R equal to 12.5 and 15 nm with the experimental data[10] (e.g., see also Table I for the latter case) we find good agreement. More generally,

the predicted behavior of the SW modes is more complicated than seen from the BLS experiments. For example, in Fig. 1(a) one can notice a "crossing" effect (with mode repulsion) of the two lowest modes near $R=12$ nm. One of these modes (label u) is the analog of the uniform mode at $k=0$, which would occur at frequency $g\mu_B 2\pi M_s \simeq 9.3$ GHz in the magnetostatic theory for cylindrical nanowires,[14] independent of the values for R and D. Its weak dependence on R in our microscopic calculations is attributed mainly to the position dependence of the dipole-dipole sums. However, a problematic feature of Fig. 1(a) is that the lowest mode is seen to go soft at the value of $R \simeq 20$ nm. This was found to be case even when we used larger r in the modeling, e.g., $r=12$ implying $N=469$, so it is a consequence of the choice of physical parameters rather than the coarseness of the numerical calculations. In relative term, the dipolar contributions may be too strong, leading to a SW instability. This leads us to reexamine the choice of D used in the calculations, which might be too small (compared to the bulk value), and also to consider the effects of single-ion anisotropy.

To investigate the dependence of the SW frequencies on the assumed value of the exchange stiffness, we have carried out calculations with other choices of D. For example, the results obtained on doubling the previous value (so $D=6.26$ T nm^2) are shown in Fig. 1(b). One can see from this figure that all the modes, except the uniform mode, are shifted up to some extent when the value of D increases. The effect of the lowest mode becoming soft is not seen in this range of radius, but the results for the SW frequencies (e.g., at $R=12.5$ and 15 nm) are no longer consistent with the experimental data.[10] Hence we go back to the original value of D, and we study the effects of nonzero single-ion anisotropy on the SW frequencies. In the present case where there is no applied magnetic field and the magnetization is along the wire axis, we assume a uniaxial form with $\mathbf{H}_{an}=(0,H_{an},0)$. The inclusion of site label n indicates that there may be a position dependence of this anisotropy, e.g., leading to a contribution to the surface pinning, and so we choose H_{an} to be $H_{a,\mathrm{surf}}$ at any surface site and to have the bulk value $H_{a,\mathrm{bulk}}$ otherwise. In Fig. 2(a) we show the results for the SW frequencies in the case where the surface anisotropy field corresponds to $H_{a,\mathrm{surf}}=0.06$ T, while the field inside the wires is $H_{a,\mathrm{bulk}}=0.02$ T. Analogous results are represented in Fig. 2(b), but choosing $H_{a,\mathrm{bulk}}=H_{a,\mathrm{surf}}=0.06$ T, so there is no contribution to the surface pinning in this case. Comparison of these with Fig. 1(a) shows that the lowest SW branch is no longer predicted to become soft in an unphysical manner. Moreover, with these relatively small anisotropy fields there is still good agreement between theory and experiment for $R=12.5$ and 15 nm. The H_{an} values are chosen arbitrarily, but we note that their magnitudes are actually comparable (or smaller) than the estimated demagnetizing field within one of the experimental samples in Ref. 10, namely, a disk-shaped sample containing $R=15$ nm nickel nanowires in an array with a filling factor of $\sim 10\%$ (by volume). Further experiments on nickel nanowires (e.g., by FMR or BLS) would be useful for a proper determination of the single-ion anisotropy fields. However, it is interesting to note that Ebels *et al.*[8] found evidence for a weak uniaxial anisotropy from their FMR studies of nickel nanowires. The magnitude was comparable to what we have assumed above.

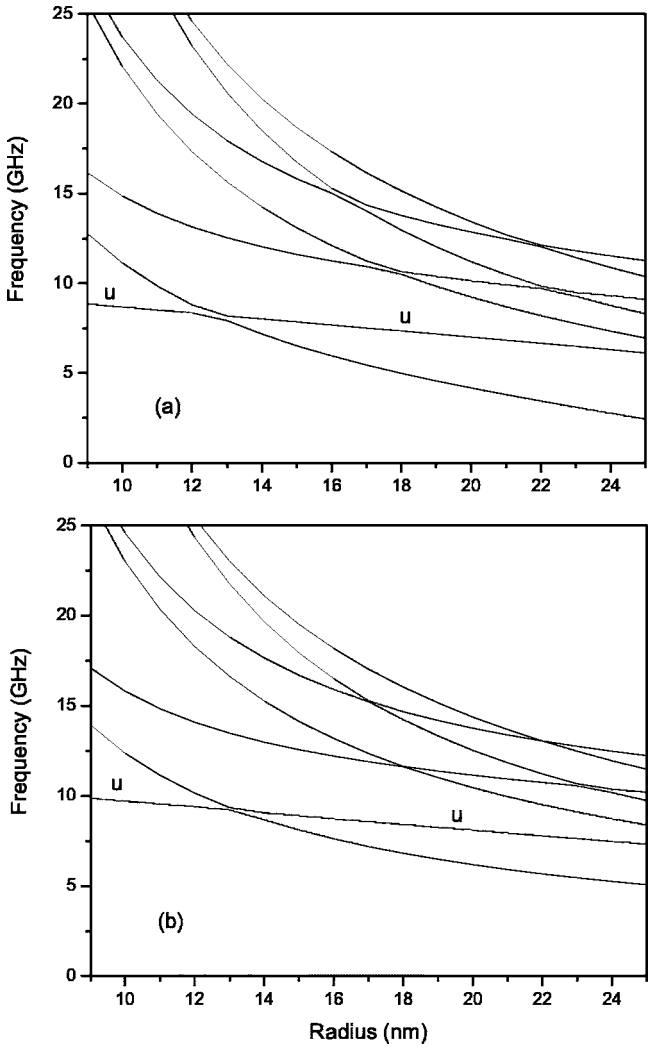

FIG. 2. SW frequency versus nanowire radius for two choices of the anisotropy fields: (a) $H_{a,\mathrm{bulk}}=0.02$ T, $H_{a,\mathrm{surf}}=0.06$ T, and (b) $H_{a,\mathrm{bulk}}=H_{a,\mathrm{surf}}=0.06$ T. The applied magnetic field is zero and $D=3.13$ T nm^2.

We now turn to the spatial dependence of the SW modes, particularly in terms of the radial parameter r_s $(=0,1,2,\ldots,r)$ introduced in Sec. II. Specifically, we have calculated for the nickel nanowires the function $D(r_s,\omega_{k,l})$ defined in Eq. (14). For each mode (with a given k and l) this quantity gives a measure of the mean squared amplitude in the "ring" of sites with radius r_s. Some numerical examples are shown in Fig. 3 for two values of $R=ra$, namely, $R=10$ and 15 nm, both modeled by taking $r=10$ as described before. The behavior is rather similar in the two cases and exhibits strong spatial effects with the occurence of nodes and antinodes, which is as expected in terms of the spatial quantization assumptions applied to the macroscopic theory in Ref. 10. The higher-frequency branches of the SW spectrum will include modes with an increasing number of nodes and/or antinodes, and the mode labeled $\omega_{k,6}$ is an example of this effect. The number of spin sites in ring r_s is equal to $6r_s$, and we note that the uniform mode [$l=1$ and $l=2$ in Figs. 3(a) and 3(b), respectively] corresponds to an approximately

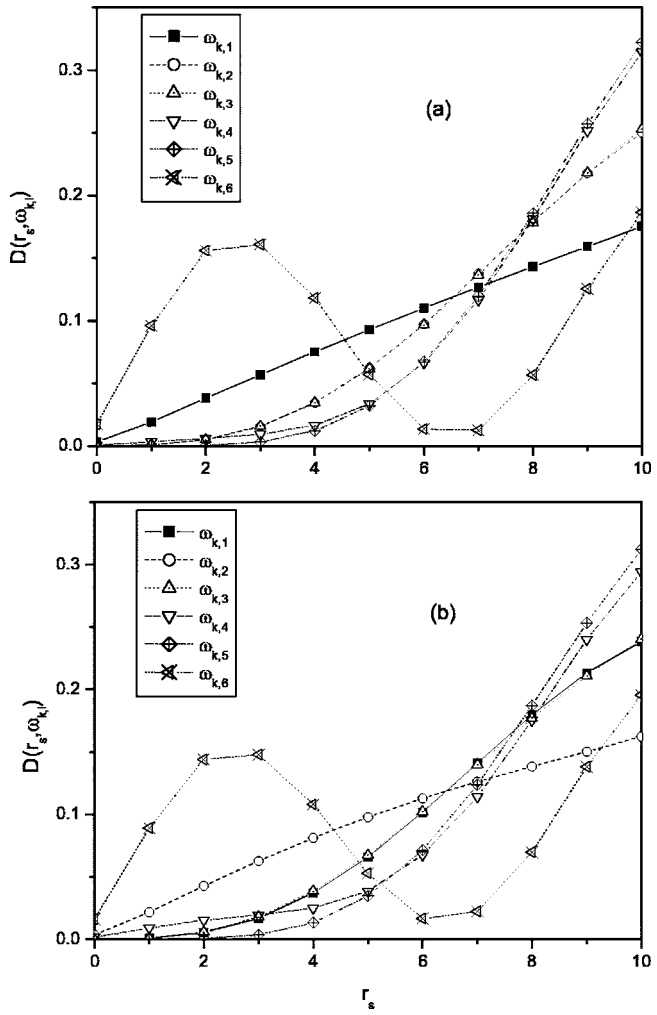

FIG. 3. Spatial distribution of the lowest six modes for R= (a) 10 and (b) 15 nm. Other parameters are chosen to be as in Fig. 1. The modes are numbered in increasing frequency.

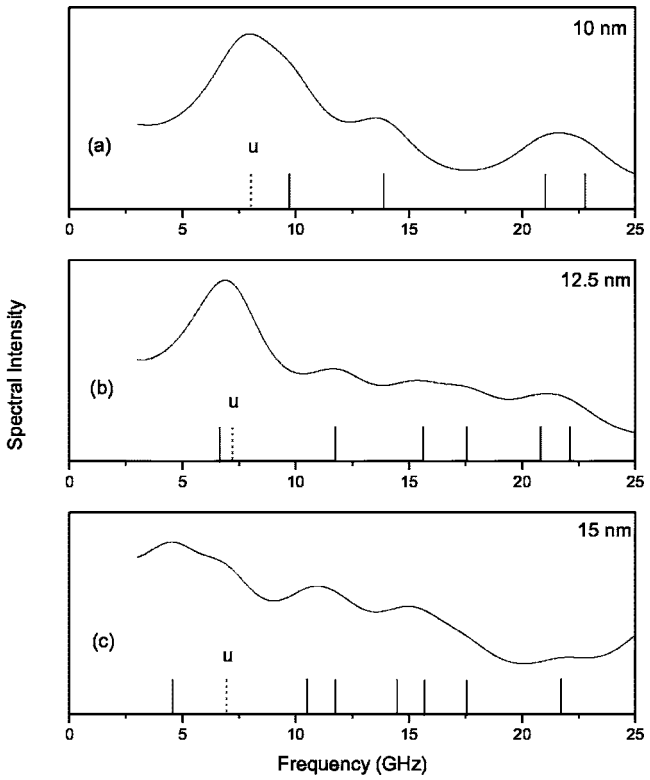

FIG. 4. Spectral intensity versus frequency for R= (a) 10, (b) 12.5, and (c) 15 nm, modeling the line shapes with ϵ=2 GHz. The short vertical lines mark the frequencies $\omega_{k,l}$ in each case.

linear increase of $D(r_s,\omega_{k,l})$ with r_s, as expected.

Next, in this zero field case, we consider the integrated intensities of the modes. These are deduced from the Green's function analysis in Eqs. (17)–(20). In the absence of damping effects, the integrated intensity $F(k,\omega)$ would consist of a series of sharp spikes (δ-function peaks) at the discrete $\omega_{k,l}$ values that we obtained earlier. In any experiment the SW modes have an intrinsic damping and also there are limitations due to instrumental resolution. Additionally, in BLS from a metal, the strong optical absorption gives rise to a spread of wave numbers and hence frequencies, the so-called "opacity broadening" effect (see, e.g., Ref. 16). In the recent BLS measurements on nickel nanowires, the three resolved peaks for the lowest SW modes when R=15 nm had a half-width ($0.5\times$full width at half maximum) of about 2 GHz (see Fig. 1 of 10). When we incorporate this phenomenologically into our theory, by replacing ω in Eq. (17) by $\omega+i\epsilon$ with ϵ=2 GHz, we obtain the results illustrated in Fig. 4. As well as the experimentally studied cases of R=12.5 and 15 nm, we have included the case of R=10 nm in order to illustrate the trend in behavior when R becomes closer to the exchange length l_{ex}. In all cases, the spectral intensity as a function of frequency shows structure due to the SW modes and, overall, there is a decrease in intensity with increasing frequency, as is the case experimentally in the BLS spectrum for the 15 nm nanowires.[10] Of course, in a more complete analysis, one would need to evaluate ϵ from first principles (by taking account of the higher-order effects contain in the Hamiltonian), and the resulting expression might depend on ω and k in general. The simple choice for ϵ made here is intended to illustrate qualitatively the lineshape effects that are produced in the experimental conditions and to estimate the relative intensities associated with the individual modes. However, apart from the above, it is important to stress that our calculated spectral intensities cannot be directly, or quantitatively, compared with the BLS spectra. The latter include factors that describe how the light enters and leaves the sample, including optical absorption effects, and takes account of the scattering process. In particular, the uniform mode does not normally contribute to the BLS spectrum, but it is included when we calculate the spectral intensities of all SW modes as in Fig. 4. It would be of interest to develop a Green's function formalism for the light scattering intensity in a nanowire (cylindrical) geometry, as has been done for the planar geometries of thin films and superlattices (see, e.g., Ref. 16), but this is currently not available. In order to give a better idea of the relative spectral intensity associated with the individual SW modes, we show in Fig. 5 the effect of reducing the half-width ϵ by a factor of 10. The relative heights of the Lorentzian-like peaks (some partially overlapping) give an indication of the individual integrated intensities, including again the uniform mode.

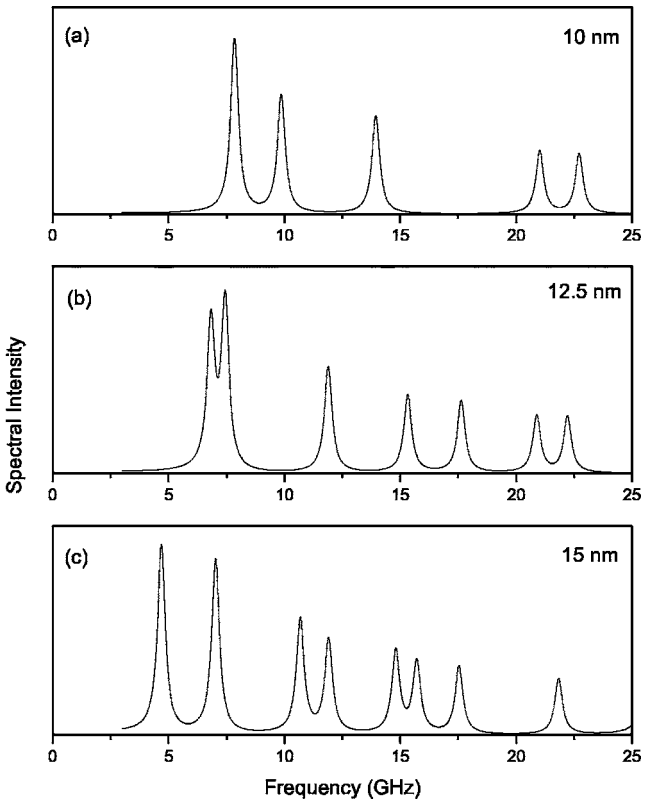

FIG. 5. Similar to Fig. 4, but with the half-width reduced to $\epsilon=0.2$ GHz.

Finally in this subsection, we discuss the effect of varying the longitudinal wave number k on the SW frequencies, since up to now we have employed the experimental value $k=0.041$ nm^{-1} from Ref. 10. Results deduced for a 15 nm nickel nanowire are shown in Fig. 6 taking, for simplicity, the other parameters to be the same as in Fig. 1(a). The k dependence is weak, as expected, in this long-wavelength regime, but we see nevertheless that there can be a subtle influence on the mode hybridization (mode repulsion) behavior for some branches.

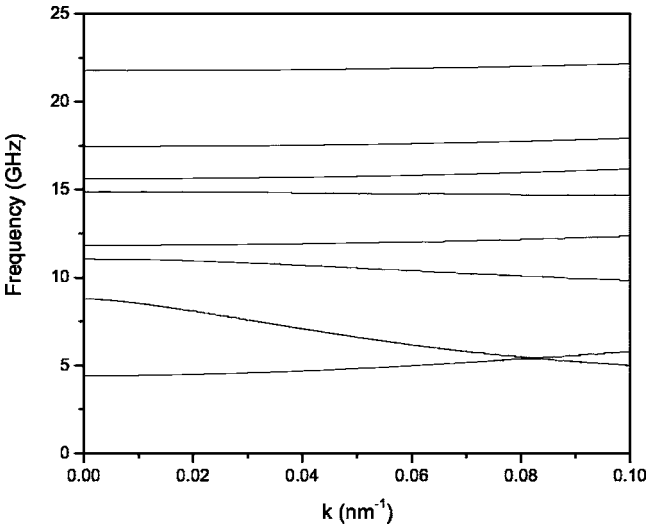

FIG. 6. SW frequency versus wave number k for a nickel nanowire with $R=15$ nm in zero applied field.

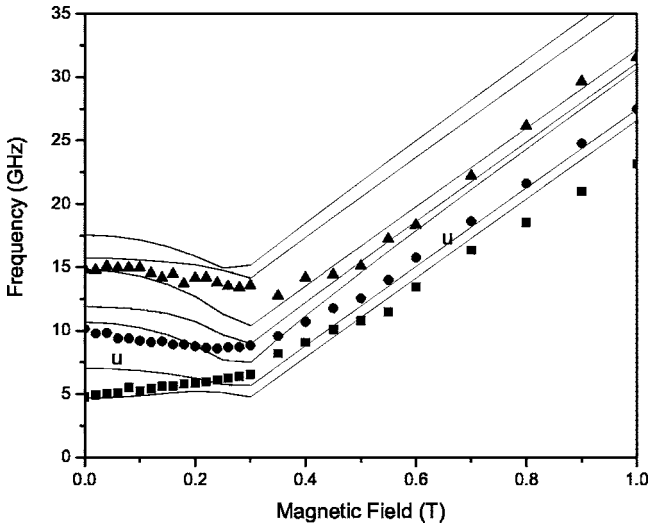

FIG. 7. Frequency versus transverse magnetic field for nickel nanowires with $R=15$ nm, taking other parameters as in Fig. 1(a). The solid curves are the theoretical results, and the symbols represent the experimental BLS data from Ref. 10.

B. Transverse applied field

We now generalize the numerical calculations to the case where there is an applied field H_0 in the transverse direction. The BLS studies on nickel nanowires in Ref. 10 corresponded to transverse fields up to 1 T, i.e., large enough to reorient the magnetization direction to lie in the transverse direction. For $H_0 \neq 0$ there is no macroscopic theory available for the SW modes, because the magnetization becomes spatially nonuniform and canted away from the wire axis.

First we calculate the SW frequencies and their spatial distributions following the procedure outlined in Sec. II. We take the case of nanowires with $R=15$ nm, modeled using effective parameters $r=10$ and $a=1.5$ nm (so $N=331$) as described before. The values of k, M_s, and D are for simplicity taken to be the same as deduced from the zero-field analysis of the BLS experiments,[10] and we ignore single-ion anisotropy effects. Some results for the lowest-frequency modes $\omega_{k,l}(l=1,\ldots,7)$ as a function of the transverse applied field are shown in Fig. 7. For comparison we also represent the experimental data (taken from the inset to Fig. 1 of Ref. 10). There are several points of interest. The transition at a field value $H_c \simeq 0.30$ T, identified in Ref. 10 as the critical field to "switch" the magnetization into the perpendicular orientation, is well produced in the theory using the assumed parameters. Next, the overall behavior of the SW modes below and above H_c is fairly successfully described. We note that our second mode (labeled u) is the "uniform" mode, and so would not be seen in BLS. While the quantitative agreement between theory and experiment is not close for larger H_0, this might be due to the choice of parameters (e.g. the neglect of single-ion anisotropy). In Fig. 8 we show some re-

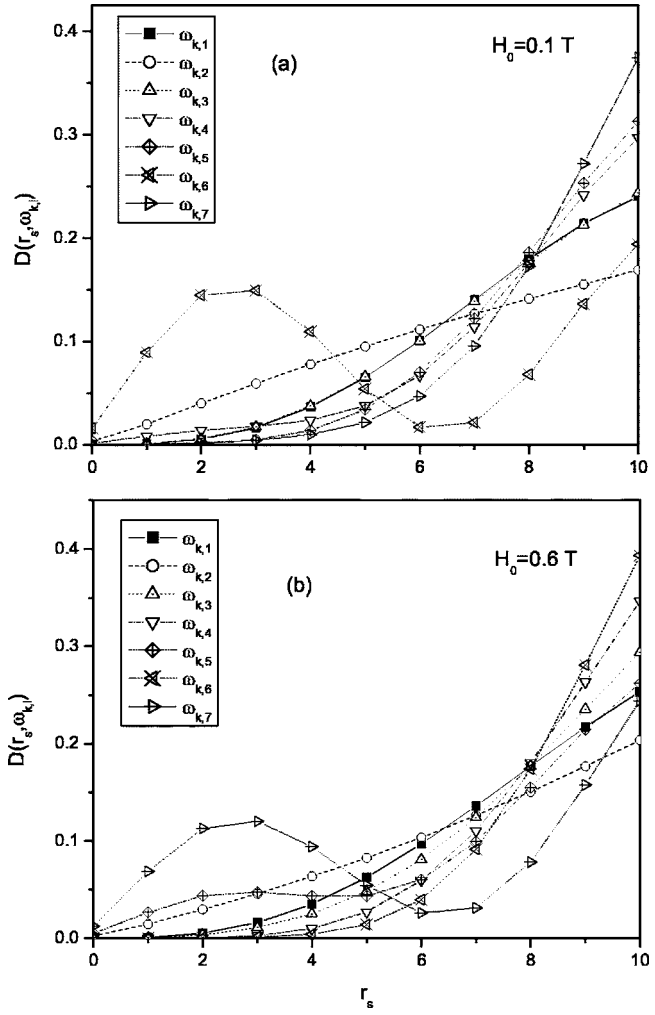

FIG. 8. Spatial distribution of the lowest seven modes for $R=15$ nm in the transverse case, taking H_0= (a) 0.1 and (b) 0.6 T.

sults for the spatial dependence of the modes for two values of H_0, chosen to be below and above the H_c value. As in Fig. 3, we plot $D(r_s, \omega_{k,l})$ versus the radial parameter r_s. Again it can be seen that some of the modes exhibit spatial resonances with the occurence of nodes and/or antinodes.

Finally, we have studied the spectral intensities of the modes, once more choosing $R=15$ nm and values of H_0 below and above H_c. In Fig. 9 the results are calculated with the half-width parameter $\epsilon=2$ GHz, chosen in accordance with the experimental data as mentioned earlier. The frequencies of the lowest three broadened peaks in each case correspond roughly to those seen experimentally,[10] although as cautioned before we have calculated spectral intensities not BLS intensities. Some similar calculations are shown in Fig. 10 but with the value of ϵ reduced to 0.2 GHz. This illustrates the spectral intensities of the individual modes more clearly.

IV. DISCUSSION AND CONCLUSIONS

We have developed our previous theoretical work[11] on the discrete dipole-exchange SW modes in ferromagnetic nanowires by extending the analysis of the spatial distribution of the modes and adding (through a Green's function analysis) results for the relative intensities and spectral line shapes of the modes. Additionally, we allowed for the inclusion of an applied magnetic field at arbitrary orientation to the cylindrical axis of the nanowires and for effects due to single-ion anisotropy (e.g., contributing to the pinning). This was done with the aim of applying the theory quantitatively to the BLS experiments on nickel nanowires reported in Ref. 10. It was particularly important to do this in the case of a transverse applied field because the macroscopic (or continuum) approach does not apply, as we discussed.

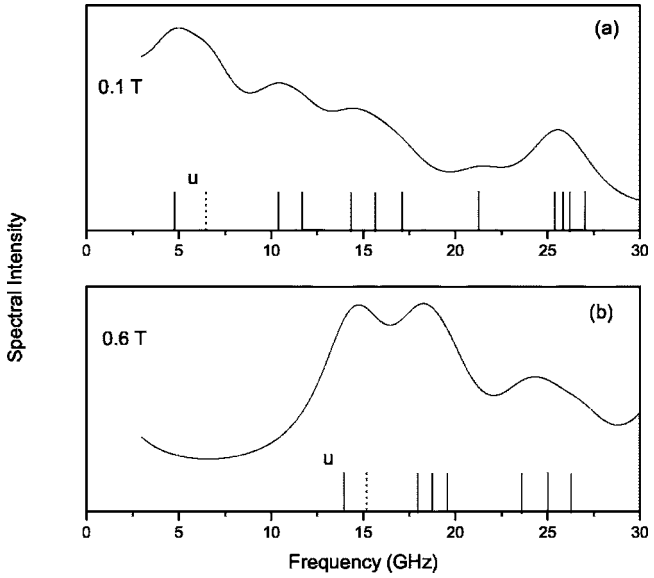

FIG. 9. Spectral intensity for $R=15$ nm calculated in the transverse case with $\epsilon=2$ GHz, taking H_0= (a) 0.1 and (b) 0.6 T.

Overall, we have shown an encouraging correspondence between our theory and the experimental data, both for $H_0=0$ and for nonzero transverse H_0. In the zero-field case

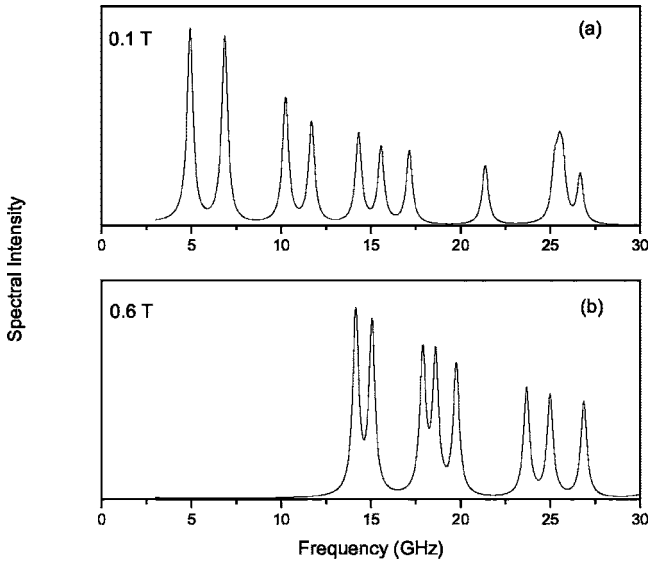

FIG. 10. Similar to Fig. 9, but with the half-width reduced to $\epsilon=0.2$ GHz.

we found that the same parameter values for M_s, D, and k as employed previously on the basis of a macroscopic analysis (with small pinning) gave good agreement with nickel nanowires for R equal to 12.5 and 15 nm, but for larger $R(\gtrsim 20$ nm) the lowest SW branch was predicted to show a soft-mode behavior. Increasing the value of the exchange stiffness D (e.g., by doubling its value to take it closer to the accepted bulk value for nickel) produced a poor fit for the frequencies of the SW modes, whereas by contrast keeping the same D value but introducing small uniaxial single-ion anisotropy could lead to satisfactory results. It would be of interest to have further experimental data on nickel nanowires (e.g., by BLS or FMR) to deduce the single-ion anisotropy in these samples. In the case of transverse H_0 (and using the same parameters) we were able to demonstrate satisfactory agreement, at least qualitatively, with the experiments on the 15 nm sample.

For both the zero-field and transverse-field cases we deduced results for the spatial distribution of intensity of the modes with respect to a radial parameter, showing evidence for nodes and/or aninodes in some cases, as postulated in Ref. 10 for the case of $H_0=0$. Results were also presented for the relative spectral intensities of the different SW modes in the case of $R=15$ nm. Qualitatively, these results showed the same features as the BLS spectra,[10] although we emphasized that there is an important quantitative difference between the two types of spectra, precluding a direct comparison. It would be of interest, in future theoretical work, to extend the formalism for light scattering intensities for planar surfaces to the cylindrical geometry of the present case. This would involve incorporating the details about how the light enters and leaves the sample (e.g., through the end of a wire or through the curved surface) and the effects of optical absorption. Finally, it would be of interest to carry out similar comparisons between our theory and BLS experimental studies for nanowire samples of other materials (such as iron and permalloy) as these become available, and this might necessitate a more detailed analysis of single-ion anisotropy effects. Some preliminary BLS data for permalloy nanowires have just been published.[19]

ACKNOWLEDGMENTS

Partial support from NSERC of Canada is gratefully acknowledged. We also thank M. H. Kuok and D. J. Lockwood for helpful discussions regarding the experimental data for nickel nanowire arrays.

APPENDIX

For arbitrary orientations of the applied and single-ion anisotropy fields the coefficients $A^{(2)}_{n,m}(k)$ and $B^{(2)}_{n,m}(k)$ in Eq. (7) are

$$\begin{aligned}A^{(2)}_{n,m}(k) = {} & \Delta_n\delta_{n,m} - \frac{1}{2}SJ_{n,m}(k)\{\cos(\theta_n-\theta_m) + \sin\alpha_n\sin\alpha_m + \cos(\theta_n-\theta_m)\cos\alpha_n\cos\alpha_m - i\sin(\theta_n-\theta_m)(\cos\alpha_n+\cos\alpha_m)\} \\ & + \frac{1}{2}(g\mu_B)^2S\{D^{x,x}_{n,m}(k)[\sin\theta_n\cos\alpha_n\sin\theta_m\cos\alpha_m + \cos\theta_n\cos\theta_m + i(\cos\theta_n\sin\theta_m\cos\alpha_m - \sin\theta_n\cos\alpha_n\cos\theta_m)] \\ & + D^{y,y}_{n,m}(k)\sin\alpha_n\sin\alpha_m + D^{z,z}_{n,m}(k)[\cos\theta_n\cos\alpha_n\cos\theta_m\cos\alpha_m + \sin\theta_n\sin\theta_m + i(\cos\theta_n\cos\alpha_n\sin\theta_m \\ & - \sin\theta_n\cos\theta_m\cos\alpha_m)] + D^{x,z}_{n,m}(k)[\sin(\theta_n+\theta_m)(\cos\alpha_n\cos\alpha_m-1) - i(\cos\alpha_n-\cos\alpha_m)\cos(\theta_n+\theta_m)] \\ & - D^{x,y}_{n,m}(k)[\sin\theta_n\cos\alpha_n\sin\alpha_m + \sin\alpha_n\sin\theta_m\cos\alpha_m + i(\cos\theta_n\sin\alpha_m - \sin\alpha_n\cos\theta_m)] \\ & - D^{y,z}_{n,m}(k)[\cos\theta_n\cos\alpha_n\sin\alpha_m + \sin\alpha_n\cos\theta_m\cos\alpha_m + i(\sin\alpha_n\sin\theta_m - \sin\theta_n\sin\alpha_m)]\}, \end{aligned} \tag{A1}$$

$$\begin{aligned}B^{(2)}_{n,m}(k) = {} & -\frac{1}{4}SJ_{n,m}(k)\{\cos(\theta_n-\theta_m)(\cos\alpha_n\cos\alpha_m-1) + \sin\alpha_n\sin\alpha_m + i(\cos\alpha_n-\cos\alpha_m)\sin(\theta_n-\theta_m)\} \\ & + \frac{1}{4}(g\mu_B)^2S\{D^{x,x}_{n,m}(k)[\sin\theta_n\cos\alpha_n\sin\theta_m\cos\alpha_m - \cos\theta_n\cos\theta_m + i(\cos\theta_n\sin\theta_m\cos\alpha_m + \sin\theta_n\cos\alpha_n\cos\theta_m)] \\ & + D^{y,y}_{n,m}(k)\sin\alpha_n\sin\alpha_m + D^{z,z}_{n,m}(k)[\cos\theta_n\cos\alpha_n\cos\theta_m\cos\alpha_m - \sin\theta_n\sin\theta_m - i(\sin\theta_n\cos\theta_m\cos\alpha_m \\ & + \cos\theta_n\cos\alpha_n\sin\theta_m)] + 2D^{x,z}_{n,m}(k)[\sin\theta_n\cos\alpha_n\cos\theta_m\cos\alpha_m + \cos\theta_n\sin\theta_m + i(\cos\theta_n\cos\theta_m\cos\alpha_m \\ & - \sin\theta_n\cos\alpha_n\sin\theta_m)] - 2D^{x,y}_{n,m}(k)[\sin\theta_n\cos\alpha_n\sin\alpha_m + i\cos\theta_n\sin\alpha_m] \\ & - 2D^{y,z}_{n,m}(k)[\sin\alpha_n\cos\theta_m\cos\alpha_m - i\sin\alpha_n\sin\theta_m]\}, \end{aligned} \tag{A2}$$

where

$$\Delta_n = g\mu_B H_{an}^{(x)} \sin\theta_n \sin\alpha_n + g\mu_B (H_{\parallel} + H_{an}^{(y)}) \cos\alpha_n + g\mu_B (H_{\perp} + H_{an}^{(z)}) \cos\theta_n \sin\alpha_n$$
$$+ \sum_l \{SJ_{n,l}(0)[\cos(\theta_n - \theta_l)\sin\alpha_n \sin\alpha_l + \cos\alpha_n \cos\alpha_l] - (g\mu_B)^2 S[D_{n,l}^{x,x}(0)\sin\theta_n \sin\alpha_n \sin\theta_l \sin\alpha_l$$
$$+ D_{n,l}^{y,y}(0)\cos\alpha_n \cos\alpha_l + D_{n,l}^{z,z}(0)\cos\theta_n \sin\alpha_n \cos\theta_l \sin\alpha_l + D_{n,l}^{x,z}(0)\sin(\theta_n + \theta_l)\sin\alpha_n \sin\alpha_l]\}. \quad \text{(A3)}$$

Here $J_{n,m}(k)$ and $D_{n,m}^{\alpha,\beta}(k)$ denote the 1D Fourier transforms with respect to k of $J_{in,jm}$ and $D_{in,jm}^{\alpha,\beta}$, respectively, and $\mathbf{H}_{an} = (H_{an}^{(x)}, H_{an}^{(y)}, H_{an}^{(z)})$ for the anisotropy field at site n.

[1] J. I. Martín, J. Nogués, K. Liu, J. L. Vicent, and I. K. Schuller, J. Magn. Magn. Mater. **256**, 449 (2003).
[2] A. Fert and L. Piraux, J. Magn. Magn. Mater. **200**, 338 (1999).
[3] *Spin Dynamics in Confined Magnetic Structures I*, edited by B. Hillebrands and K. Ounadjela (Springer-Verlag, Berlin, 2002).
[4] S. O. Demokritov, B. Hillebrands, and A. N. Slavin, Phys. Rep. **348**, 441 (2001).
[5] K. Nielsch, F. Müller, A. P. Li, and U. Gösele, Adv. Mater. (Weinheim, Ger.) **12**, 582 (2000).
[6] K. Nielsch, R. B. Wehrspohn, J. Barthel, J. Kirschner, U. Gösele, S. F. Fischer, and H. Kronmüller, Appl. Phys. Lett. **79**, 1360 (2001).
[7] A. Encinas-Oropesa, M. Demand, L. Piraux, I. Huynen, and U. Ebels, Phys. Rev. B **63**, 104415 (2001).
[8] U. Ebels, J. L. Duvail, P. E. Wigen, L. Piraux, L. D. Buda, and K. Ounadjela, Phys. Rev. B **64**, 144421 (2001).
[9] D. H. Reich, M. Tanase, A. Hultgren, L. A. Bauer, C. S. Chen, and G. J. Meyer, J. Appl. Phys. **93**, 7275 (2003).
[10] Z. K. Wang, M. H. Kuok, S. C. Ng, D. J. Lockwood, M. G. Cottam, K. Nielsch, R. B. Wehrspohn, and U. Gösele, Phys. Rev. Lett. **89**, 027201 (2002).
[11] T. M. Nguyen and M. G. Cottam, Phys. Rev. B **71**, 094406 (2005).
[12] R. N. Costa Filho, M. G. Cottam, and G. A. Farias, Phys. Rev. B **62**, 6545 (2000).
[13] J. M. Pereira and M. G. Cottam, Phys. Rev. B **68**, 104429 (2003).
[14] T. M. Sharon and A. A. Maradudin, J. Phys. Chem. Solids **38**, 977 (1977).
[15] R. Arias and D. L. Mills, Phys. Rev. B **63**, 134439 (2001).
[16] M. G. Cottam and D. J. Lockwood, *Light Scattering in Magnetic Solids* (Wiley, New York, 1986).
[17] J. R. Sandercock and W. Wettling, J. Appl. Phys. **50**, 7784 (1979).
[18] K. Y. Guslienko and A. N. Slavin, Phys. Rev. B **72**, 014463 (2005).
[19] H. Y. Liu, Z. K. Wang, H. S. Lim, S. C. Ng, M. H. Kuok, D. J. Lockwood, M. G. Cottam, K. Nielsch, and U. Gösele, J. Appl. Phys. **98**, 046103 (2005).